Assessment of the Impact of Long Integration Time in Geosynchronous SAR Imagery of Agricultural Fields by Means of GB-SAR Data

Albert Aguasca, *Member, IEEE*, Antoni Broquetas, *Member, IEEE*, Juan M. Lopez-Sanchez, *Senior Member, IEEE*, Xavier Fàbregas, *Member, IEEE*, Jordi J. Mallorqui Franquet, *Senior Member, IEEE*, and Mireia Mas

***Abstract*—Geosynchronous synthetic aperture radar (GeoSAR) missions offer the advantage of near-continuous monitoring of specific regions on Earth, making them essential for applications that require continuous information. However, wind-induced motion along the inherent long integration time can result in image defocusing, with potential degradation of retrieved information. This article aims to investigate the impact of GeoSAR long integration time in synthetic aperture radar (SAR) imaging and derived products (time series of backscatter and coherence) required to extract agriculture-relevant soil or crop parameters of interest. The study is based on the extensive HydroSoil data acquisition campaign carried out over barley and corn crops, funded by the European Space Agency. The collected raw data are used to synthesize equivalent apertures with integration times of up to 4 h, similar to those acquired with a GeoSAR. These ultraslow apertures facilitate the assessment of the impact of agricultural scene decorrelation on the generation of images with extended integration times.**

***Index Terms*—Backscattering, coherence amplitude, geosynchronous synthetic aperture radar (GeoSAR), integration time, scene decorrelation.**

I. Introduction

GLOBAL warming, as a result of climate change, increases the rate of water evaporation worldwide [1], [2], with an impact on the seas and continents, increasing the likelihood of extreme weather events, such as floods or droughts that directly affect agricultural production. For that reason, science drivers call for persistent observations of the water cycle, which can be reached from satellites by using geosynchronous orbits (GEO) and microwave sensors. Radars in low Earth orbit (LEO) satellites give relatively poor coverage at mid and low latitudes (e.g., Africa) with revisiting times from days to weeks. In contrast, synthetic aperture radars (SAR) in GEO satellites (GeoSAR) would provide much more flexible imaging with shorter revisit times. Different GeoSAR missions are currently being studied [3], [4], recently a GeoSAR L-band mission has been launched from China with a spatial resolution of 20 m [5] and new ones could emerge soon. All of them propose innovative mission concepts that offer a remarkable range of capabilities that would have a significant impact on the sciences of weather forecasting and hydrology. In addition, they would provide direct benefits to society. An example is the study of the diurnal water cycle, with an impact on the rapid development of intense storms or the changes in soil moisture/surface wetness during the day.

The data acquisition and processing with geosynchronous radars [6] significantly differ from classical LEO systems. One of the main differences is the long integration times required for acquiring an image, from seconds in LEOs to minutes or even hours in GEOs with different compromises of achieved spatial and temporal resolutions [7]. Different problems of GeoSAR missions are being studied such as the development of high gain deployable reflectors able to compensate for the huge two-way propagation losses, or the proposal of innovative techniques for precise orbit determination above the GNSS satellite navigation constellations [8]. In addition, the long GeoSAR acquisition times make the scene decorrelation, among other factors, a potential key constraint that requires further investigation using experimental data, which is the focus of this article.

The ESA-funded HydroSoil measurement campaign [9], [10] provided a massive amount of data in an agricultural scenario simulating the frequent acquisitions of the Hydroterra mission [11]. The objective of the HydroSoil campaign was to demonstrate the retrieval of soil moisture and vegetation parameters in an agricultural field under controlled conditions using a ground-based fully-polarimetric SAR instrument. The massive collected SAR data of the campaign have been used to generate apertures equivalent to those from a GeoSAR. These equivalent apertures are perfectly suited for assessing the performance and limitations of the previously mentioned GeoSAR systems in

Manuscript received 20 September 2023; revised 6 November 2023; accepted 23 November 2023. Date of publication 1 December 2023; date of current version 14 December 2023. This work was supported in part by the European Space Agency (ESA Contract 4000132509/20/NL/FF/ab with UPC) and in part by the Spanish MCINN funds Unidad de Excelencia Maria de Maeztu MDM-2016-0600, under Project PID2020-117303GB-C21/AEI/10.13039/501100011033, and under Project PID2020-117303GB-C22/AEI/10.13039/501100011033. *(Corresponding author: Albert Aguasca.)*

Albert Aguasca, Antoni Broquetas, Xavier Fàbregas, Jordi J. Mallorqui Franquet, and Mireia Mas are with the CommSensLab, Department of Signal Theory and Communications, Universitat Politècnica de Catalunya, E08034 Barcelona, Spain (e-mail: alberto.aguasca@upc.edu; antoni.broquetas@upc.edu; francisco.javier.fabregas@upc.edu; jordi.joan.mallorqui@upc.edu; mireia.mas.mendez@upc.edu).

Juan M. Lopez-Sanchez is with the University Institute for Computer Research (IUII), University of Alicante, E-03690 Alicante, Spain (e-mail: juanma.lopez@ua.es).

Digital Object Identifier 10.1109/JSTARS.2023.3338468

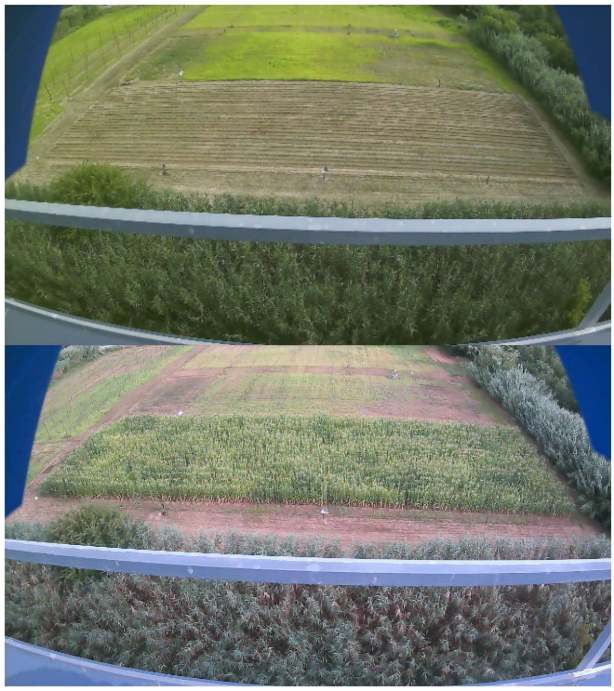

Fig. 1. Photographs taken from the radar site showing the agricultural field in two stages of the corn campaign. (Top) Bare soil with deployed drip irrigation (July 15, 2020). (Bottom) Fully grown corn (August 23, 2020).

a controlled environment. Two measurement campaigns were carried out with two different crops, barley from March 2020 to June 2020 and corn from July 2020 to November 2020. The radar data were acquired by a fully automated FM-CW C-band ground-based SAR (GB-SAR) developed by UPC's CommSensLab specifically for the HydroSoil test field. The measurement campaign of the two crops, despite the constraints and limitations imposed by the COVID pandemic, has enabled access to several months of continuous monitoring of the agricultural field with a temporal resolution of 10 min and a spatial resolution of around 2 m^2 over a scenario of 22 $\times$ 60 m^2, as shown in Fig. 1. Both campaigns have resulted into a huge dataset of more than 31 000 polarimetric acquisitions which were complemented with intensive additional in-field ancillary data, as soil roughness, soil moisture, plant density, leaf area index, biomass, and local meteorological information.

This article presents the results of combining and processing this vast amount of data to assess the performance of GeoSAR imagery, characterized by its long integration time, to provide relevant information for hydrology and agricultural applications. This is achieved by means of a suitable subaperture combination of fast-acquisition raw data to create equivalent ultraslow (US) radar apertures. The performance of GeoSAR imagery in the retrieval of biophysical variables are aspects outside the scope of this manuscript which were partially considered during the preparatory studies of the Hydroterra mission.

This article is structured as follows. In Section II, the test site, the instrument, and the main details of the experimental campaigns are presented. Section III describes how the equivalent US apertures are generated from a set of fast acquisitions.

Fig. 2. GB-SAR instrument is deployed on the roof of the EEABB building, pointing to the experimental agricultural field.

Section IV presents the metrics used to evaluate and validate the proposed method of generating equivalent GeoSAR apertures. In Section V, data analysis and discussion, based on the backscatter and coherence evolution, are applied to confirm the capability of GeoSAR systems to provide relevant information from long integration time SAR apertures with short revisiting times. Finally, Section VI concludes this article.

II. Experiment Description: Location, Instrumentation, and Data Processing

The test site of the HydroSoil campaign is the experimental agricultural field of the Barcelona School of Agricultural Engineering (EEABB), Universitat Politècnica de Catalunya at 41°16'36"N 1°59'11"E. The cultivated area size is 22 m $\times$ 60 m (depth and width), and it is located 25 m far from the facade of the EEABB building. The GB-SAR is mounted on its roof, as shown in Fig. 2, centered with respect to the crop area. The incidence angles of the radar in the test field are constrained by the geometry, ranging from 50° at near range to 65° at far range. Notably, the incidence angle of a GeoSAR like Hydroterra would be in a similar range (45°–60°) over Europe, so it is representative of acquisitions of such a GeoSAR system. Various corner reflectors and dihedrals tilted 0° and 45° with respect to the vertical direction have been deployed for the radiometric and polarimetric calibration of the radar images.

The main instrument is a C-band ground-based full-polarimetric SAR (GB-PolSAR). A set of pyramidal horn antennas, two in transmission and two in reception, are used as radiation elements. The transmitting antennas are oriented to transmit with horizontal (H) and vertical (V) polarizations, respectively. Receiving antennas follow the same strategy. The radar electronics are thermally stabilized with a tolerance of <1 °C to minimize gain and phase drifts. The main parameters of the radar system are listed in Table I.

The radar was normally operated with a temporal baseline (TB) of 10 min, providing a convenient sampling given the expected dynamics of agricultural scenes. This parameter was chosen as a good compromise between the capability of providing

TABLE I
RADAR MAIN PARAMETERS

Parameter	Value
Central Frequency (Bandwidth)	5.6 GHz (200 MHz)
Modulation	Saw-Tooth FM-CW
Chirp PRF	338.5 Hz
Receiver Noise Figure	2 dB
3dB Antenna Beam-width	60° (Az.), 40° (El.)
Aperture length (rail speed)	1.47 m (1 m/s)
Integration time	1.47 s
Radar acquisition interval	10 min

a reliable continuous operation, the mechanical specifications and tolerable wear of the linear motion unit, and the amount of generated data.

A backprojection algorithm (BPA) has been used to focus the single look complex (SLC) images resulting in a tolerable computational cost given the moderate scene size [12]. The BPA has been selected because it offers a high degree of flexibility in focusing extended images from arbitrary synthetic apertures limited by either antenna beam, linear track, or data acquisition capability.

To obtain accurate backscattering measurements the antenna patterns have been measured in an anechoic chamber and compensated in the SAR processor. In addition, the radar electronics have been characterized for the whole radar bandwidth in the laboratory before on-site installation. From the known radar cross-section of the stable reflectors deployed next to the observed field, the backscattering data has been calibrated with an error below 1 dB.

III. EQUIVALENT ULTRASLOW APERTURE GENERATION

Operating the GB-SAR in a US acquisition mode for directly obtaining long integration datasets, in the order of hours, was discarded since it was not compatible with the campaign requirement to maintain a continuous SAR data acquisition with a constant 10-min observation period. Despite that, the assessment of long-integration-time synthetic apertures is performed in this work by a suitable combination of multiple raw-data subapertures taken from normally operated fast GB-SAR data acquisitions. In this way, equivalent US apertures have been obtained with integration times up to 4 h, which are suitable to study the impact of SAR long integration times on image quality.

When the radar is operated in the normal fast aperture mode (hereafter FAST), a set of FM-CW chirps are sequentially transmitted along the rectilinear trajectory for each transmitting polarization, H and V, whereas the two receiving channels, H and V, simultaneously measure the polarimetric radar response. With the current GB-SAR configuration, the synthesized aperture length is around 1.4 m, with a measurement aperture time of 1.4 s. The SLC imagery is obtained by processing the raw data with an optimized BPA [8]. The time interval between consecutive apertures, the TB, can be set as desired according to the aforementioned mechanical limitations. For the experimental campaigns, it was set to 10 min.

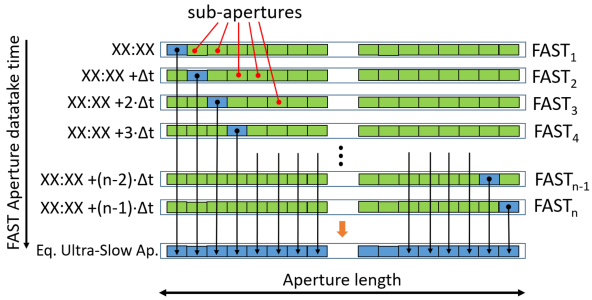

Fig. 3. Set of n subapertures of the raw data of consecutive normally operated GB-SAR apertures are combined to generate an equivalent US aperture, as the one generated by GeoSAR systems. Δt is the TB of consecutive FAST acquisitions.

The equivalent US aperture for a defined total aperture interval time is built by combining subapertures of consecutive FAST apertures, acquired during the desired time span. For this purpose, a block with a fixed number of consecutive chirp responses of each aperture is placed in its corresponding time slot of the equivalent US aperture, and this procedure is repeated for all FAST apertures used to build the US aperture, as shown in Fig. 3. To generate a US aperture from the fast ones, with the same parameters in terms of spatial sampling and transmitted energy, a total amount of 240 chirps have to be combined along the 1.4 m aperture length.

During the corn campaign, the radar was operated with a TB of 10 min. Nonetheless, on certain dates during the whole campaign and for a short period of time, the TB was reduced to 2 min.

Assuming an initial set of fast apertures with a TB of 2 min and taking only two chirp responses from each one, 120 subapertures are required to form a US one with an aperture time of 240 min. This total integration time of 4 h can be considered the worst-case scenario of analysis as the potential impacts of scene decorrelation are maximized.

In this case, each segment of two consecutive chirps from a fast acquisition represents only 0.83% of the 240 chirps of the final aperture, which is small enough to guarantee a realistic decorrelation along the data acquisition time, as in the case of a long aperture interval time. This US aperture type, formed with 2-min TB FAST acquisitions is named US2 hereafter.

Similarly, in the case of managing a set of apertures with a TB of 10 min, the 4-h equivalent aperture is built by taking segments of 10 chirp responses from consecutive apertures. Each segment of 10 chirps represents an occupation of only 41% of the overall aperture time. This US aperture type is named US10.

Those chirps from the US aperture obtained from the same FAST aperture exhibit a higher correlation than those belonging to different FAST apertures. For US2, the impact of having two chirps from the same FAST aperture can be considered insignificant in terms of decorrelation reduction with respect to a real aperture of the same long integration time. In the case of US10, there are groups of 10 chirps from the same FAST aperture, so a priori it is difficult to foresee its impact. This point will be studied in Section IV.

US apertures with shorter integration time could be generated by combining a smaller number of subapertures, but the number

of chirp responses from each FAST acquisition should be higher. Increasing the number of chirp responses taken from the same FAST acquisition would raise the correlation among them and, thus, might reduce the decorrelation effects associated with long integration times that would be observed in an actual GeoSAR image. Obviously, the impact would depend on the particular characteristics of the scene. For instance, an agricultural field or a forest scene decorrelates faster than an urban area.

IV. Evaluation of the Equivalent US Apertures

This section addresses the impact of the way the US aperture is formed upon the realism or the fidelity of the obtained image. Considering that an identical duration of the US aperture is set, the differences will be driven by the TB of the FAST acquisitions, which determines the length (or number of chirps) of the subapertures taken from each acquisition.

The vast majority of FAST apertures acquired during the campaign had a TB of 10 min, so the derived US apertures employed to assess the resulting GeoSAR imagery have been restricted to the equivalent ones with 4 h integration time, i.e., the US10.

The method to validate the US10 as a representative US aperture consists of the comparison of US10 and US2 images generated from the same dataset of FAST apertures. The following premise is applied: if US apertures built from FAST aperture segments taken every 2 min (US2) are assumed to be equivalent to nominal US apertures, with a pulse repetition interval of 1 min. Then, if a US aperture built from segments taken every 10 min (US10) provides similar values (in the comparison metrics), it can be concluded that such a US10 aperture can be considered as an equivalent GeoSAR system aperture.

For this study, the following three cases are being considered and compared: FAST, US10, and US2, the first with an integration time of 1.4 s and the two later with equivalent integration times of 4 h. Most of the data to be used for the validation were acquired on September 21, 2020, with a mean wind speed of 2.7 m/s. Fig. 4 shows the SLCs obtained after processing the three different datasets taken on September 21, 2020. The cultivated area is identified by the red polygon, whereas the green ones indicate areas covered with reeds. The white polygons mark areas with no controlled crops. Although the three images are very similar, some differences are evident.

The FAST SLC defines clear and sharp transitions between vegetated and low reflectivity or shadowed areas, which have been highlighted in Fig. 4 with orange polygons. In contrast, the US10 and US2 images show blurred transitions. At the same time, the two strong scatterers, which correspond to corner reflectors deployed for calibration purposes, look very similar in the three cases as, in principle, they are not affected by temporal decorrelation. The former are distributed scatterers, which partially belong to vegetated areas that decorrelate faster, whereas the latter are deterministic ones, which behave as persistent scatterers and are more immune to decorrelation phenomena. This different behavior can be explained by the long-aperture time and the impact of the wind on a vegetated scenario. The effect is an equivalent cross-range defocusing of the response

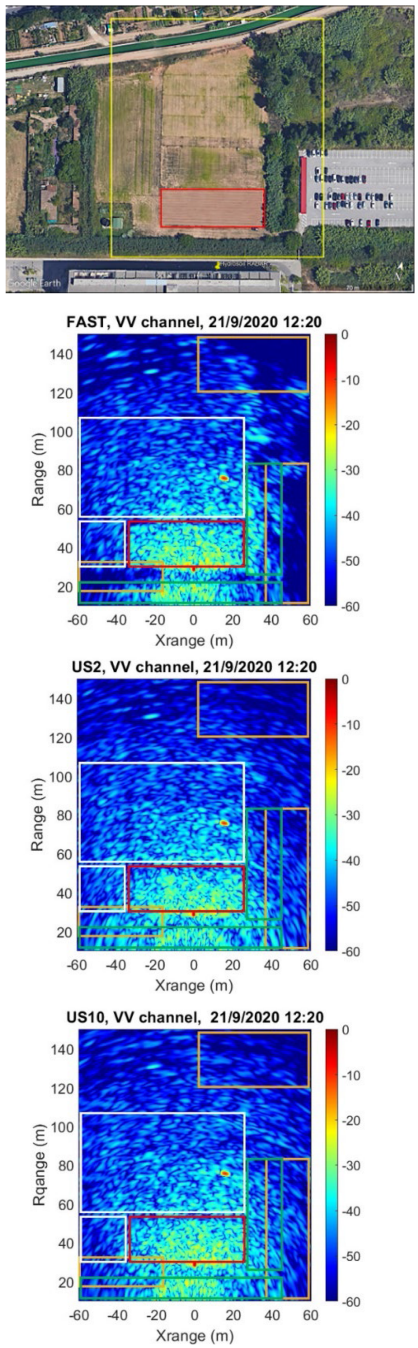

Fig. 4. From top to bottom, Google Earth image (6/2020) of the field and surroundings. FAST pol-VV SLC image in radar coordinates taken at 12:20. US2 pol-VV SLC image for the period 10:20–14:18. US10 pol-VV SLC image for the period 10:20–14:18. All SLC images are normalized to the same maximum backscattering σ°. Two calibrators can be clearly seen at cross-range/range coordinates (0,29) and (16,76) m. The cultivated area is identified by the red polygon, whereas the green ones indicate areas covered with reeds. The white polygons mark areas with no controlled crops.

of high-reflectivity areas around them [12]. The wind-induced motion decreases the correlation among the received backscattering signals from different radar azimuth positions. Thus, the defocusing worsens the quality of the resulting image when the aperture integration time increases.

Different metrics have been used to compare the performance of the FAST and US apertures and evaluate the validity of the US as a good representation of those images that would be acquired by GeoSAR systems. The metrics exploited are as follows.

1) Image resolution analysis at point targets (corner reflectors).
2) Image energy from its autocorrelation.
3) Complex correlation coefficient of SLC pairs.
4) Normalized sum of squared differences (SSD) among SLCs' pairs.

These metrics evaluate and compare different parameters of the FAST and the equivalent US apertures to measure the image quality and characterize the degradation inherent to longer acquisition times. It must be noted that the image degradation, primarily its spatial resolution, is not uniform because it depends on the scene.

A. Image Resolution at Point Targets

The image of stable calibration point targets should exhibit the same point spread function and spatial resolution for FAST and US acquisitions. The effective sensor parameters can be considered identical in all three cases, at least in terms of energy, range, and azimuth sampling rates and theoretical resolutions. At the same time, a corner reflector behaves as a point scatter that presents a very stable behavior along time, insensitive to the presence of winds and, thus, does not decorrelate along time. Therefore, the spatial resolution measured at the locations of the corner reflectors deployed in the scene (for calibration purposes) should be identical in all cases.

The first reflector is a 50 cm leg triangular-faced trihedral deployed at polar radar coordinates of 36.2 m in range and 1° in cross-range (an equivalent cross-range of 0.7 m in Cartesian radar coordinates at that range). The second reflector is a vertically oriented 40 cm leg dihedral at 76 m in range and 12° in cross-range (equivalent to 16 m in Cartesian coordinates). Their response can be clearly seen in the SLCs of Fig. 4 as bright spots.

The range and cross-range cuts of the SLC images around the corner reflector are shown in Fig. 5 for two different wind situations: calm (wind speed below 0.5 m/s) and windy (5 m/s wind speed). No differences between the FAST and US10 apertures are found, despite the difference in wind conditions that could alter their surroundings and modify how the clutter affects their response. Due to the electrical size of the reflectors, their backscattered power is much higher than the one from the surrounding clutter. The resolution is estimated around 0.75 m in range and 1.1° in cross-range for both corner reflectors.

B. Image Energy

The second parameter to be considered for evaluating the validity of the equivalent US apertures is the energy of the image since, ideally, the aperture time should not affect it.

The maximum of the autocorrelation of an SLC image corresponds to its energy [13]. The values obtained for the different types of apertures are compared. This parameter is obtained for the same observed area and corresponds to the whole cultivated field, denoted with a red rectangle in the top image of Fig. 4. The area under study does not include any corner reflector.

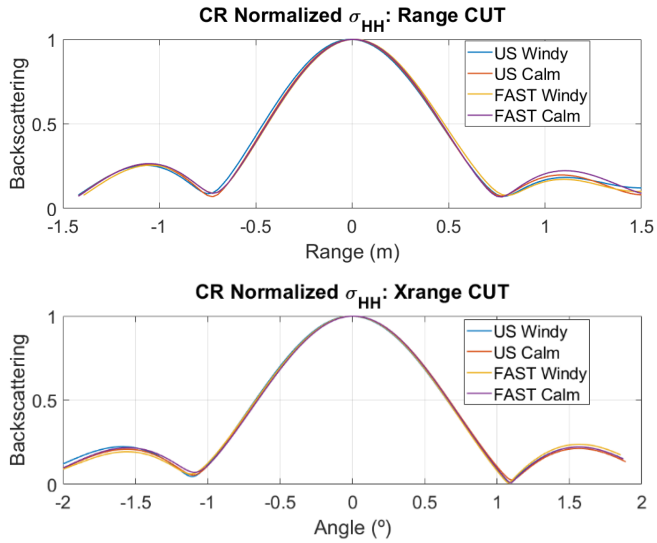

Fig. 5. (Top) Range and (bottom) cross-range cuts of the normalized HH radar backscattering of the triangular-shaped trihedral of FAST and US10 apertures. Windy stands for 5 m/s wind speed, whereas calm denotes a wind speed below 0.5 m/s.

TABLE II
MAXIMUM VALUES OF THE AUTOCORRELATION OF THE HH-POL SLC

POL SLC	
Type of aperture	*Normalized Autocorrelation / (dB)*
FAST of vegetated scenario, 21/9/2020 (8:20h)	1 / (0 dB) Reference
US2. of vegetated scenario, 21/9/2020 (8:20-12:18h)	1.005 / (0.021 dB)
US10. of vegetated scenario, 21/9/2020 (8:20-12:10h)	0.994 / (-0.026 dB)
FAST of bare soil, 22/6/2020 (7:40h)	0.172 / (-7.644 dB)
US10. of bare soil, 22/6/2020 (11:50-15:50h)	0.174/ (-7.594 dB)

Table II shows the maximum autocorrelation of the HH-pol SLC images over the selected vegetated area, normalized to the same reference value (the measure obtained for a FAST SLC). As it can be seen, both kinds of US apertures show similar values compared with the FAST one for the same scenario. It can be concluded that the combination of segments of FAST apertures produces similar results for both US2 and US10 strategies in terms of the resulting image energy. In addition, the energy values obtained at a date in which the area was bare soil (June 22, 2020) are included in Table II. As it can be expected, the energy at the bare soil acquisition is noticeably lower than the fully-grown crop acquisition, but the values at FAST and US10 are also virtually equal.

C. Complex Correlation Coefficient: Interimage Coherence

The complex correlation coefficient is a measure of the strength of the linear relationship between two sets of data. When

TABLE III
COHERENCE MAGNITUDE FOR PAIRS OF HH CHANNEL SLCS FOR THE FIELD UNDER STUDY

Pair of SLCs	Coherence at 6:20AM sept. 21, 2020 (wind: 0.8 m/s)	Coherence at 12:00PM sept. 21, 2020 (wind: 3 m/s)
FAST SLCs, 2 min. between apertures	0.9861	0.8521
FAST SLCs, 4 h. between apertures	0.6691	0.7762
FAST and US2	0.8723	0.7499
FAST and US10	0.8580	0.7132
US10 and US2	0.9581	0.8733

managing two zero-mean complex SAR images I_1 and I_2, this coefficient is known as complex coherence, and is defined as [14]

$$\gamma = \frac{E\{I_1 I_2^*\}}{\sqrt{E\left\{|I_1|^2\right\} E\left\{|I_2|^2\right\}}} \tag{1}$$

where E $\{\cdot\}$ is the expectation operator.

The coherence magnitude $|\gamma|$ in (1) is a parameter between 0 and 1. Small values of $|\gamma|$ indicate that the images I_1 and I_2 are uncorrelated with each other, whereas for values close to 1 there is a high correlation between the two images. A key advantage of this metric is that it also considers the phase differences among the images.

In practice, assuming ergodicity and stationarity over a particular area of the image, the expectation can be replaced by spatial averaging. In that case, the estimated coherence $\hat{\gamma}$ can be calculated as follows:

$$\hat{\gamma} = \frac{\sum_{i=0}^{L} p(i)_{\text{image1}}\, p(i)^*_{\text{image2}}}{\sqrt{\sum_{i=0}^{L} \left|p(i)_{\text{image1}}\right|^2 \sum_{i=0}^{L} \left|p(i)_{\text{image2}}\right|^2}} \tag{2}$$

where $p(i)_{\text{image1}}$ and $p(i)_{\text{image2}}$ are the pixels of the SLC images for the same position in the area and L is the number of averaged pixels or number of looks. The larger the number of looks the more reliable will be the estimation of the coherence but at a lower spatial resolution.

The amplitude of the coherence can be used to detect and characterize differences or similarities in pairs of US10, US2, and FAST SLCs. This coefficient is calculated first for the following pairs of images, a pair of FAST SLCs acquired with a TB of 2 min and also with 4 h between them (see Table III). The table also includes the results for the following pairs of simultaneous SLCs, FAST versus US2, FAST versus US10, and US2 versus US10. With the first two pairs, the expected figures for the nominally operated SAR are defined. The following three values can be compared with respect to the nominal one to confirm the validity of the US10 aperture. This set of coefficients are obtained for two different instants of the same day with different mean wind speeds 0.8 and 3 m/s (see Fig. 6). The reference FAST aperture for US comparison is selected at the mid-integration time of the US aperture.

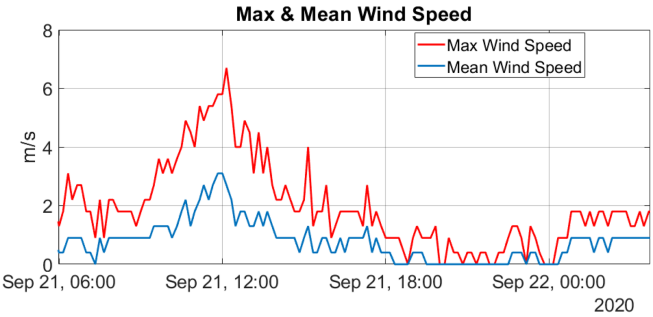

Fig. 6. Mean and maximum wind speed profile for the period September 21 and 22, 2020.

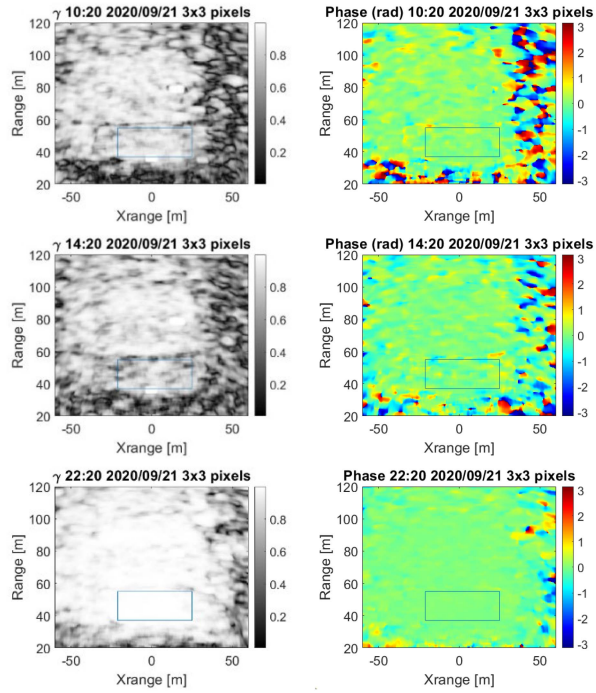

Fig. 7. Coherence magnitude (left column) and phase difference map (right column) of pairs of US2 and US10 images at different times of the day (10:20, 14:20, and 22:20).

According to Table III, FAST versus US2 and FAST versus US10 show similar figures. In contrast, the pair US10 versus US2 shows a higher value. This result can be expected due to the similarity of both apertures, since there is a large number of common chirps (subapertures) used in both of them.

If we have a closer look at the difference between US2 and US10 we can further validate its behavior depending on the environmental conditions. Fig. 7 shows the amplitude and phase of the complex coherence maps for a L of 3×3 looks (three independent pixels in range and theee in cross-range) between US2 and US10 at three different moments of the day: 10:20, 14:20, and 22:20 for an extended area beyond the field under study. The areas with no or low vegetation preserve the coherence amplitude and phase for both cases. On the contrary, the areas with trees are affected by heavy decorrelation as seen on the right part of all images. The higher decorrelation is closely linked to the higher wind speeds along the day, (see Fig. 6). As

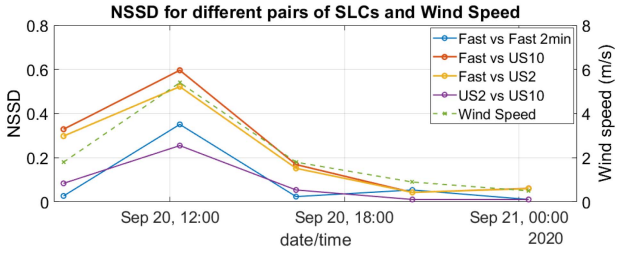

Fig. 8. Normalized SSD for different pairs of SLC along the day. The different wind conditions ease to evaluation of the quality of the US apertures. The pairs Fast versus US10 and Fast versus US2 show similar values for every wind condition while the pairs of two fast SLCs separated 2 min or US10 versus US2 have reduced NSSD due to the similarity between them.

at night, the wind speed significantly decreased, the coherence raised in the trees area. For the area under study (marked by the polygon in Fig. 7) the phase standard deviation is 6.1°, 7.31°, and 1.28° for 10:20, 14:20, and 22:20 data taken apertures.

D. Normalized Sum of Squared Differences

The SSD is another similarity metric. It is a statistical measure of deviation from the mean, also known as variation, and characterizes the match between two images based on the intensity differences between them. It is calculated from the summation of the squared subtraction, pixel by pixel, of two images. Usually, this figure is normalized (NSSD) by the images' energy as

$$\text{NSSD} = \frac{\sum_{\text{pixels}} |p_1 - p_2|^2}{\sqrt{\sum_{\text{pixels}} |p_1|^2 \cdot \sum_{\text{pixels}} |p_2|^2}}. \tag{3}$$

The lower the value of NSSD the more similar are the two images. Two identical images will give NSSD equal to zero. In this case, the NSSD is applied between different SLCs for the same date (September 21, 2020) when the crop was fully grown and different wind conditions occurred. The area under study is limited to the agricultural field of the experiment. First, the value of NSSD for pairs of FASTs is calculated and used as a reference value. According to Fig. 8, a direct impact of the wind speed upon NSSD is found, with the lowest values in the evening and at night.

If the NSSD values are calculated and analyzed for different pairs of SLCs, it can be concluded that the NSSD for pairs of FAST versus US2 apertures are similar to the ones for FAST versus US10 apertures regardless of the wind conditions.

As a result of considering these different metrics for evaluating and comparing the different types of apertures, it can be concluded that the equivalent 4-h US aperture generated by means of combining segments of consecutive fast apertures with an aperture repetition time of 10 min (US10) can be considered representative of long integration time GeoSAR apertures.

V. Data Analysis and Discussion

In the previous section, it has been demonstrated the capability of obtaining US apertures from consecutive acquisitions of FAST ones. The applicability of these slow aperture data to agricultural monitoring is preliminarily confirmed in this section. Time series of backscattering and coherence can be used to characterize the temporal variations of soil moisture, crop stage, biomass, etc. [15], [16], [17]. Some of these applications are still in an early stage, but the preliminary results are really promising. A GeoSAR sensor could provide data with short revisit intervals (hours), hence expanding the current applications based on the use of LEO satellites with revisit times of several days. The data collected during the HydroSoil campaign has allowed us to relate the temporal evolution of fast aperture data with the different parameters. The comparison of the backscattering and coherence evolution of slow and fast aperture images shows a good agreement. Therefore, the similar behavior found confirms the capability of GeoSAR systems to provide relevant and useful information for agricultural applications with an enhanced refresh rate.

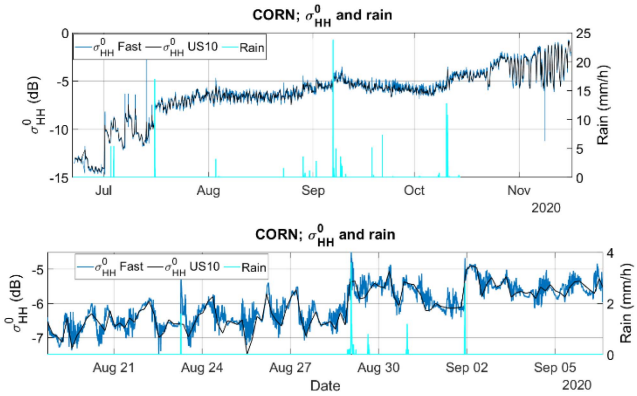

Fig. 9. Long-term backscattering evolution of the HH channel for the corn crop. (Top) $\sigma^\circ_{\text{HH}} \frac{\partial^2 \Omega}{\partial v^2}$ increases as the plants grow. (Bottom) A zoom of the σ°_{HH} evolution shows a daily fluctuation while the rain episodes force a step response.

A. Backscattering Evolution

When monitoring agricultural fields with SAR imagery, radar backscattering can be used to detect and characterize not only the soil moisture variations but also the crop stage. For this reason, the long-term backscattering evolution along the whole growing season is analyzed and compared for both kinds of apertures to detect any anomalous performance in US10 images.

Fig. 9 shows, for both approaches, the HH backscattering evolution during more than 4 months of the corn campaign. The date and time of the different rain episodes are highlighted in blue as well as its intensity in mm/h.

Fig. 9 shows that the time series of the backscattering coefficient (σ°) time series provided by FAST and US10 present extremely similar behaviors, being the latter a low-pass version of the former. At the beginning of the period, some peaks of σ^0 can be distinguished that are caused by irrigation events. At the end of the cultivation period, high amplitude fluctuations with a daily period can be observed that should be caused by a strong reduction of the plant water content, when the husks and many leaves are no longer green because the crop reached the maturity stage [18] and the main backscattering mechanism could be affected by the dew on leaves. Such fluctuations are common to

both FAST and US10, but the longer aperture duration of US10 produces a smoother behavior of its backscattering time-series.

These results can be extrapolated to the other polarimetric channels and polarimetric observables (e.g., target decomposition outputs).

B. Coherence Evolution

With the proper selection of the number of looks, the coherence between two SAR images is an excellent quantitative change indicator with sensitivity to vegetation biophysical variables [19].

When a time series of N SAR images $I(t)$ is available, a multitemporal coherence matrix Γ can be defined as [20]

$$\Gamma = \begin{bmatrix} 1 & \gamma_{12}\ \gamma_{13} & \cdots & \gamma_{1N} \\ \vdots & & \ddots & \vdots \\ \gamma_{N1} & & \cdots & 1 \end{bmatrix}. \tag{4}$$

Any element of the matrix in (4) is the complex coherence, as defined in (1), for a pair of images. The element γ_{ij} is

$$\gamma_{ij} = \frac{E\left\{I\left(t\right) I^{*}\left(t+\Delta t\right)\right\}}{\sqrt{E\left\{\left|I\left(t\right)\right|^{2}\right\} E\left\{\left|I\left(t+\Delta t\right)\right|^{2}\right\}}} \tag{5}$$

where Δt is the TB length between images i and j and, as presented before, these elements can be estimated using a spatial averaging with the selected multilook (2). For this study and considering that the cultivated area includes a homogeneously distributed target, the number of looks or independent resolution cells has been estimated in the order of 900.

The coherence magnitude is obviously symmetric $|\gamma_{ij}| = |\gamma_{ji}|$. The impact of the length of the TB in the coherence can be analyzed from the k-diagonal terms of the matrix, where $k = 0$ is the main diagonal of the matrix (or equivalently a zero TB. For a given k, all terms have the same TB, which is k times the minimum one (4 h for US10 data).

For this analysis, the following TBs between images have been selected: 4 h (minimum baseline as in case of two consecutive US apertures), 12 h, 24 h, and 6 days (as the revisiting time for LEO orbital SAR systems, e.g., Sentinel-1).

Fig. 10 shows the temporal evolution, for the selected TB lengths, of the coherence magnitude of the HH polarization for the whole area under study, of FAST and US10 apertures. The results can be extrapolated to the other polarimetric channels.

An expected degradation of the coherence is clearly seen as the TB is increased. High values of coherence are obtained for shorter TBs, with a daily fluctuation in both kinds of apertures due to the atmospheric activity during the diurnal part of the day. It is obvious that no significant difference between both kinds of apertures can be observed.

Fig. 11 shows the scatter plot that relates pairs of FAST and US coherence values belonging to the same time. It has to be mentioned that the FAST coherence times are centered with respect to the US ones. The graphs include the 0.05 absolute error limits. The total amount of pairs is above 800 for each TB.

To qualitatively evaluate the resemblance between the two approaches, the difference between the coherences derived from

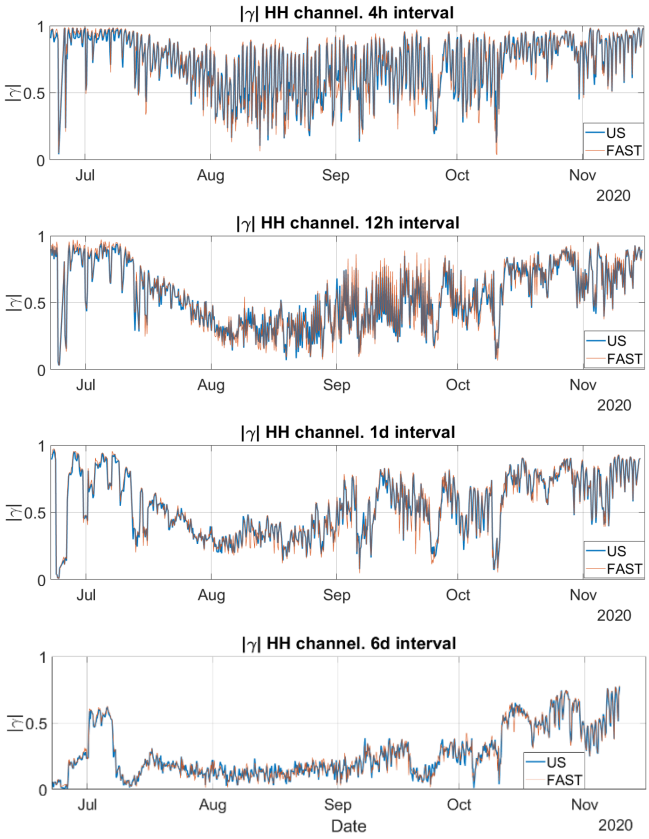

Fig. 10. HH channel coherence evolution of FAST and US10 apertures. From top to bottom, time series of 4 h, 12 h, 1 day, and 6 days TB.

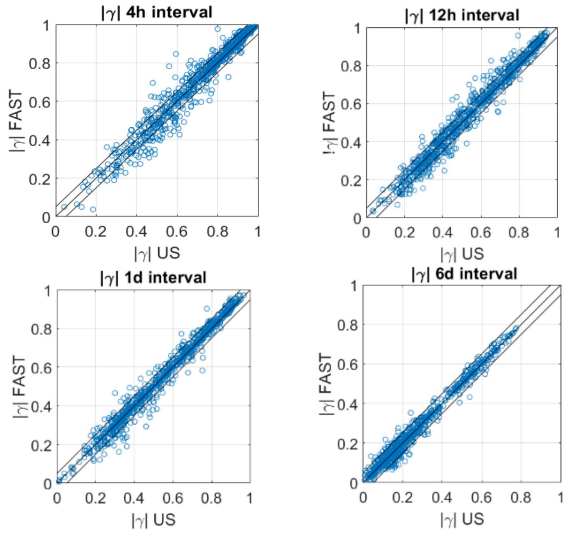

Fig. 11. Scatter plot of FAST versus US10 HH channel coherence. From top left to bottom right time series of 4 h, 12 h, 1 day, and 6 days TB. The coordinates of every circle are the corresponding US (X-axis) and FAST (Y-axis) coherence amplitudes belonging to the same time.

FAST and US acquisitions can be used as

$$e_{\gamma} = \left|\left|\gamma_{\mathrm{FAST}}\right| - \left|\gamma_{\mathrm{US}}\right|\right| \ . \tag{6}$$

TABLE IV
RELATIVE NUMBER OF PAIRS, IN %, FOR AN ABSOLUTE ERROR e_γ BELOW 0.05 FOR THE DIFFERENT TIME BASELINES

Temporal baseline	$e_\gamma \leq 0.05$
4 hours	80.3
12 hours	80.4
1 day	88.2
6 days	92.2

Results are summarized in Table IV, where the difference dispersion is quantified by means of the relative number of pairs with an error e_γ <0.05. This term is above 80% for any TB.

VI. CONCLUSION

In this article, a study of the feasibility of the use of slow data acquisitions of GeoSAR missions have been carried out by means of the HydroSoil campaign data, where a C-band GB-SAR was employed to monitor, among other information, the crop evolution in a controlled agricultural field. SAR acquisitions equivalent to data gathered from 4-h integration time have been constructed by taking small consecutive subapertures of multiple acquisitions along the 4-h virtual data take. First, the equivalent US apertures have been evaluated to confirm their feasibility by means of different metrics. Second, once the subapertures have been combined to obtain the equivalent GeoSAR raw data, the US SLC images have been assessed in comparison with short aperture time images showing no relevant differences, in terms of spatial resolution and energy, with respect to a conventional normal data-take.

If the temporal evolution of the backscattering and coherence obtained by the two methods are compared, it can be concluded that both datasets show similar performances. This result confirms the feasibility of obtaining information from GeoSAR images of agricultural areas under typical moderate wind conditions, showing the potential of retrieving valuable information related to soil moisture and vegetation parameters.

The presented study has evaluated the impact of agricultural scene decorrelation on long aperture GeoSAR missions. Other potential problems of GeoSAR missions such as limited signal-to-noise ratio, precise orbit determination, the impact of atmospheric phase screen on the image and derived products cannot be properly assessed with the presented results [21] and should be evaluated with complementary studies [8].

REFERENCES

[1] E. Olmedo et al., "Increasing stratification as observed by satellite sea surface salinity measurements," *Sci. Rep.*, vol. 12, 2022, Art. no. 6279.

[2] R. Kramer et al., "Evapotranspiration trends over the eastern United States during the 20th century," *Hydrology*, vol. 2, pp. 93–111, 2015.

[3] S. Hobbs et al., "G-CLASS: Geosynchronous radar for water cycle science - orbit selection and system design," *J. Eng.*, vol. 2019, pp. 7534–7537, Nov. 2019. [Online]. Available: https://doi.org/10.1049/joe.2019.0601

[4] S. Hobbs et al., "G-CLASS: Geosynchronous radar for water cycle science – orbit selection and system design," *J. Eng.*, vol. 2019, pp. 7534–7537, 2019.

[5] A. Jones, "China launches first geosynchronous orbit radar satellite," *SpaceNews*, Aug. 14, 2023. [Online]. Available: https://spacenews.com/China-launches-first-geosynchronous-orbit-radar-satellite/, Accessed: Nov. 2023.

[6] J. R. Rodon, A. Broquetas, A. M. Guarnieri, and F. Rocca, "Geosynchronous SAR focusing with atmospheric phase screen retrieval and compensation," *IEEE Trans. Geosci. Remote Sens.*, vol. 51, no. 8, pp. 4397–4404, Aug. 2013.

[7] S. Hobbs and A. Monti-Guarnieri, "Geosynchronous continental land-atmosphere sensing system (G-Class): Persistent radar imaging for Earth science," in *Proc. IEEE Int. Geosci. Remote Sens. Symp.*, 2018, pp. 8621–8624.

[8] J. Nicolás-Álvarez et al., "Interferometric orbit determination system for geosynchronous SAR missions: Experimental proof of concept," *Remote Sens.*, vol. 14, 2022, Art. no. 4871.

[9] European Space Agency, "HydroSoil - ESA earth online," European Space Agency, Paris, France. [Online]. Available: https://earth.esa.int/eogateway/campaigns/hydrosoil, Accessed: Nov. 2023.

[10] A. Aguasca et al., "Hydrosoil, soil moisture and vegetation parameters retrieval with a C-band GB-SAR: Campaign implementation and first results," in *Proc. IEEE Int. Symp. Geosci. Remote Sens.*, 2021, pp. 6685–6687.

[11] J. C. Calvet et al., *Report for assessment: Earth Explorer 10 Candidate Mission Hydroterra European Space Agency*, Noordwijk, The Netherlands, ESA-EOPSM-HYDR-RP-3779, 2020.

[12] M. Lort, A. Aguasca, C. López-Martínez, and X. Fàbregas, "Impact of wind-induced scatterers motion on GB-SAR imaging," *IEEE J. Sel. Topics Appl. Earth Observ. Remote Sens.*, vol. 11, no. 10, pp. 3757–3768, Oct. 2018.

[13] A. Carlson, *Communication Systems*, 3rd ed. Singapore: McGraw-Hill, 1986.

[14] I. Cumming and F. Wong, *Digital Processing of Synthetic Aperture Radar Data: Algorithms and Implementation*. Norwood, MA, USA: Artech House, 2005.

[15] N. Mira, J. Catalao, G. Nico, and P. Mateus, "Soil moisture estimation using atmospherically corrected C-band InSAR data," *IEEE Trans. Geosci. Remote Sens.*, vol. 60, 2022, Art. no. 4505609.

[16] A. Mestre-Quereda, J. M. Lopez-Sanchez, F. Vicente-Guijalba, A. W. Jacob, and M. E. Engdahl, "Time-series of Sentinel-1 interferometric coherence and backscatter for crop-type mapping," *IEEE J. Sel. Topics Appl. Earth Observ. Remote Sens.*, vol. 13, pp. 4070–4084, 2020.

[17] C. Silva-Perez, C. Marino, J. M. Lopez-Sanchez, and I. Cameron, "Multi-temporal polarimetric SAR change detection for crop monitoring and crop type classification," *IEEE J. Sel. Topics Appl. Earth Observ. Remote Sens.*, vol. 14, pp. 12361–12374, 2021.

[18] L. Abendroth, R. Elmore, M. Boyer, and S. Marlay, "Corn growth and development," Iowa State Univ. Extension, Ames, IA, USA, Rep. PMR1009, 2011.

[19] A. Villaroya-Carpio, J. Lopez-Sanchez, and M. Engdahl, "Sentinel-1 interferometric coherence as a vegetation index for agriculture," *Remote Sens. Environ.*, vol. 280, Oct. 2022, Art. no. 113208.

[20] A. Jacob et al., "Sentinel-1 InSAR coherence for land cover mapping: A comparison of multiple feature-based classifiers," *IEEE J. Sel. Topics Appl. Earth Observ. Remote Sens.*, vol. 13, pp. 535–552, 2020.

[21] L. Iannini and A. M. Guarnieri, "Atmospheric phase screen in ground-based radar: Statistics and compensation," *IEEE Geosci. Remote Sens. Lett.*, vol. 8, no. 4, pp. 537–541, May 2011.

Albert Aguasca (Member, IEEE) was born in Barcelona, Spain, in 1964. He received the M.Sc. and Ph.D. degrees in telecommunication engineering from the Universitat Politecnica de Catalunya (UPC), Barcelona, Spain, in 1989 and 1993, respectively.

Since 1995, he has been an Associate Professor with the School of Telecommunications Engineering, UPC. His teaching activities involve RF and microwave circuits for communications and radio navigation systems. He has published more than 40 papers on microwave SAR, radiometer systems, and microwave circuits. His research interests include the design and development of SAR and microwave radiometer systems for unmanned aerial vehicle platforms.

Antoni Broquetas (Member, IEEE) was born in Barcelona, Spain, in 1959. He received the M.Sc. degree in telecommunication engineering and the Ph.D. degree in telecommunications engineering (microwave tomography) from the Universitat Politecnica de Catalunya (UPC), Barcelona, Spain, in 1985 and 1989, respectively.

In 1986, he was a Research Assistant with Portsmouth Polytechnic, Portsmouth, U.K., involved in propagation studies. In 1987, he joined the Department of Signal Theory and Communications (TSC), UPC. From 1998 to 2002, he was a Subdirector of Research with the Institute of Geomatics, Barcelona, Spain. Since 1999, he has been a Full Professor with UPC involved in research on radar imaging and remote sensing. From 2003 to 2006, he was a Director of the TSC Department at UPC. He has authored more than 150 papers on microwave tomography, radar, ISAR and SAR systems, SAR processing, and interferometry.

Juan M. Lopez-Sanchez (Senior Member, IEEE) was born in Alicante, Spain, in 1972. He received the Ingeniero (M.S). and Doctor Ingeniero (Ph.D.) degrees in telecommunication engineering from the Technical University of Valencia, Valencia, Spain, in 1996 and 2000, respectively.

From 1998 to 1999, he was a predoctoral grantholder with the Space Applications Institute, Joint Research Centre of the European Commission, Ispra, Italy. Since 2000, he has led the Signals, Systems, and Telecommunication Group of the University of Alicante, Alicante, Spain, where he has been a Full Professor since 2011. He has coauthored 115 papers in refereed journals and more than 160 contributions to international conferences and symposia. His research interests include microwave remote sensing for inversion of biophysical parameters, polarimetric and interferometric techniques, and applications of radar remote sensing in agriculture and geophysics.

Dr. Lopez-Sanchez was the Chair of the Spanish Chapter of the IEEE Geoscience and Remote Sensing Society from 2006 to 2012. He was the recipient of the Indra Award for the best Ph.D. thesis on radar in Spain in 2001.

Xavier Fàbregas (Member, IEEE) received the B.S. degree in physics from Barcelona University, Barcelona, Spain, in 1988, and the Ph.D. degree in applied sciences from the Universitat Politecnica de Catalunya (UPC), Barcelona, Spain, in 1995.

In 1990, he joined the Photonic and Electromagnetic Engineering Group, Signal Theory and Communications Department, UPC. Since 1996, he has been an Associate Professor with UPC. In 2001, he spent an 8-month sabbatical with the HR Institute of the German Aerospace Agency, Oberpfaffenhofen, Germany. From 2013 to 2016, he was the Deputy Director of Industry Relations with the Barcelona School of Telecommunications Engineering, UPC. His research activity during recent years has been focused on terrestrial SAR systems and their PolDInSAR applications for the monitoring of natural risks, i.e., deformation of land, urban areas, and rockfall, and multidimensional Speckle models PolSAR/PolInSAR in SAR images and the study of the viability of GeoSAR systems to continuous monitoring of the dynamics of the water cycle. He has authored 35 articles in journals indexed in the JRC and 136 papers presented at international and national conferences and holds 1 patent.

Jordi J. Mallorqui Franquet (Senior Member, IEEE) was born in Tarragona, Spain, in 1966. He received the M.Sc. and Ph.D. degrees in telecommunications engineering from the Universitat Politecnica de Catalunya (UPC), Barcelona, Spain, in 1990 and 1995, respectively.

Since 1993, he has been an Assistant Professor with the School of Telecommunications Engineering of Barcelona, UPC, where he became an Associate Professor in 1997, and has been a Full Professor since 2011. From 2018 to 2021, he was the Head of the Signal Theory and Communications Department, UPC. His teaching activity involves microwaves, radio navigation systems, and remote sensing. In 1999, he spent a sabbatical year with the Jet Propulsion Laboratory, Pasadena, CA, USA, where he was involved with interferometric airborne synthetic aperture radar (SAR) calibration algorithms. He has authored or coauthored more than 120 papers on microwave tomography, EM numerical simulation, SAR processing, interferometry, and differential interferometry in refereed journals and international symposia. His research interests include the application of SAR interferometry to terrain-deformation monitoring with orbital, airborne/UAV, and ground-based sensors, vessel detection and classification from SAR images, and 3-D electromagnetic simulation of SAR systems.

Mireia Mas was born in Barcelona, Spain, in 1997. He received the B.Sc. degree in telecommunication technologies and services engineering with a specialization in telecommunication systems and the M.Sc. degree in telecommunication engineering with a specialization in antennas, microwaves, and photonics for communications and earth observation from the Universitat Politecnica de Catalunya (UPC), Barcelona, Spain, in 2019 and 2021, respectively.

Since 2020, she has been involved with interferometry and polarimetry (related to her Ph.D. thesis), when she started collaborating with the HydroSoil crop radar observation campaign run by the UPC, funded by the European Space Agency. Since October 2021, she has been a part of the Ph.D. program with the Department of Signal Theory and Communications, UPC.